

Modeling of Multiterminal HVDC Offshore Grids with Renewable Energy and Storage Integration by Opensource Tools

Joachim Espvik
*Department of Electric
Power Engineering,
Norwegian University of
Science and Technology*
Trondheim, Norway
joachim_espvik@hotmail.com

Erling Vatn Tranulis
*Department of Electric
Power Engineering,
Norwegian University of
Science and Technology*
Trondheim, Norway
erling.v.t@gmail.com

Santiago Sanchez Acevedo
*Energy Systems
SINTEF Energy Research*
Trondheim, Norway
santiago.sanchez@sintef.no

Elisabetta Tedeschi
*Department of Electric
Power Engineering,
Norwegian University of
Science and Technology*
Trondheim, Norway
elisabetta.tedeschi@ntnu.no

Abstract—With increasing offshore wind penetration levels, more secure and flexible offshore electrical transmission systems are needed to ensure security of supply to onshore users. When considering long distances of electrical power transmission, HVDC grids based on the modular multilevel converter (MMC) are a solution for present and future large scale offshore wind integration. As HVDC grids are developing into large and complex systems, dynamic analyses are useful to gain knowledge on the interactions between the different components in the grids. This paper uses the open source tool OpenModelica as modeling environment to demonstrate the potential of the tool in modeling such HVDC systems. A three-terminal HVDC system with offshore wind and energy storage integration is implemented in OpenModelica, and the dynamics of the system are investigated through four simulation cases. The main focus of this paper is dynamics and operation related to the HVDC system. The simulation results show that the MMCs can improve the most rapid power fluctuations using its internal storage capabilities, while an external energy storage system provides a more constant power flow over more extensive periods, in addition to improving the operation of the HVDC system. All models used in this paper are made publicly available to anyone for any purpose, including future studies of larger HVDC grids.

Index Terms—Offshore wind power, Energy storage system, Multiterminal HVDC, MMC, Open source, OpenModelica, Dynamic modeling, Transient simulations

I. INTRODUCTION

Over the last 10 years, the installed capacity of offshore wind power has dramatically increased from 1 to 18 GW in Europe [1]. Furthermore, projections of future installation levels coupled with economic considerations and maritime spatial planning predict increasing distances to shore of future offshore wind farms [2], [3]. When transporting electrical energy in submarine cables over such long distances, economic and technical considerations make high-voltage direct current (HVDC) the preferred choice for electrical power transmission [4].

This work was partly funded by the Norwegian Research Council and DNV-GL through the NFR contract n. 250493 - within the Integrated approach to the Design and Control of Offshore HVDC Networks (IDeCON) project.

As the number of wind farms with HVDC connections to shore increases, the power system also becomes increasingly dependent on secure power supply through these HVDC connections. To ensure security of supply from these wind farms, it is useful to connect the HVDC terminals in an offshore HVDC grid [5]. This increases the flexibility of the system, as power flows in HVDC grids can be rerouted through different paths to shore. This allows power transfer from the wind farms to shore even if one of the HVDC connections is out of operation, thus, increasing the reliability of the system.

In such HVDC grids, the modular multilevel converter (MMC) is becoming the preferred power electronic converter for converting between AC and DC due to its many benefits [6]. The MMC is capable of reversing the power flow without reversing the polarity of the DC voltages by DC current reversal. Additionally, features like modularity and scalability make the MMC advantageous compared to other voltage source converter (VSC) topologies. The MMC also has an inherent capability of storing energy internally in the converter [7], which can benefit the system in which it is connected.

Another crucial aspect for offshore wind power integration is the varying power production due to the intermittency in wind speed. The varying power production from wind farms can be classified into three categories [8]. The first being the most rapid variations due to, e.g., wind gusts on the time scale of seconds. The second variation is short-term variations on the scale of minutes to hours while the third and last variation is seasonal variations. To meet this challenge, an energy storage system can be integrated into the HVDC grid to complement the power production from the offshore wind farms and further improve the overall system.

However, because HVDC grids are developing into large and complex systems with many different components, it is useful to test the system to gain knowledge on the interactions between the various components. Investigating the dynamics and testing the controllers of such large systems at full-scale is not directly feasible. Therefore, hardware-in-the-loop

(HIL) testing is often used to test HVDC grids in laboratory environments [9]. HIL combines software based simulation models that replicate the behavior of the physical components with actual physical components.

The Modelica modeling language is a tool especially used in the automobile industry for HIL testing [10], [11]. An emerging tool based on the Modelica language is OpenModelica, which is open-source and allows integration of models developed in different physical domains. Additionally, OpenModelica supports the Functional Mock-up Interface (FMI) standard that allows models developed in OpenModelica to be shared across multiple platforms and tools, and be used in, e.g., HIL testing. This makes the modeling of an HVDC grid in OpenModelica a timely investigation area, including possibilities for laboratory testing and verification.

In this paper, a model of a three-terminal HVDC grid with offshore wind and energy storage integration, including MMCs, HVDC cables, wind farms, and an energy storage system, is analyzed and implemented in OpenModelica. The topic of energy storage integration in the HVDC grid is investigated using simulations of the system to demonstrate the potential of the open source tool in such analyses. Additionally, the internal storage capabilities of the MMC are studied to investigate how the MMC can contribute to the HVDC grid support compared to an external offshore energy storage system.

As an additional contribution to the knowledge community, all models introduced in the paper are made publicly available to anyone for any purpose through the following URL: <https://github.com/joachimesp/OpenModelica-HVDC-NTNU>. Additionally, an MMC model and a point-to-point HVDC model built for Opal-RTs real-time simulator, ePHASORSIM, are added to the folder for illustration purposes on how to build models for the real-time simulator. This allows models to be used in future laboratory experiments with HIL testing.

Further details of the models developed and test cases presented hereafter can be found in [12], [13].

The remainder of the paper is organized as follows: Section II introduces the OpenModelica software with the description of a preliminary assessment of its performance. Next, Section III describes the three-terminal HVDC system with all models used to build the system. Section IV introduces the different simulation cases, their purpose, and results. Section V includes a discussion and Section VI concludes.

II. THE OPENMODELICA SOFTWARE

The Modelica modeling language is a vendor-independent standard, thus there exists multiple implementations of modeling tools using the modeling language, such as Dymola, MathModelica and IDA. However, these implementations are not open source, which makes OpenModelica an emerging tool.

One of the features used in this paper was the use of electrical components in the built-in standard library of OpenModelica. This reflects the acausal modeling approach in the software, meaning dynamics of an electrical circuit can be

modeled by drawing the circuit with circuit components and not with generic blocks as in causal modeling.

Preliminary tests were carried out to verify that OpenModelica is able to capture high frequency dynamics in the range of several kilohertz. This was done by building two 10kHz 2L-VSC models, one in OpenModelica and one in MATLAB Simulink to compare their results. The tests showed that the captured dynamics of the two models were very similar [12], [13]. Since such dynamics are of significantly higher frequency than the simulations in this paper, it was assumed that OpenModelica could accurately capture all dynamics of interest.

III. SIMULATION SYSTEM DESCRIPTION

The final goal of this paper is to investigate the dynamics of the system in fig. 1 by implementing it in OpenModelica. The topology is chosen because it is the system with the lowest complexity that allows studying the interactions between the key components in an HVDC grid, including an energy storage system.

The system in fig. 1 includes two wind farms, WF1 and WF2, three HVDC MMC converters connected by two HVDC cables and an energy storage system (ESS) connected near WF2.

WF1 consists of 70 turbines with a rated power of 7MW each, while WF2 consists of 60 turbines with a rated power of 7MW each. Both cables are of 100km length. The rated values of the energy storage will be dimensioned in simulation case 2 later in the paper. A table with all the key parameters used in the different models is included in the Appendix. For further details on the controller parameters used in this paper, the reader can refer to the appendices in [12], [13].

The models used for each component are presented in this section.

A. Energy-based MMC model

As explained in the introduction, the MMC is one of the key components in an HVDC grid, and it is used for converting between AC and DC in the grid. Figure 2 shows a schematic of the circuit of the MMC that is built of multiple submodules. Each submodule is, in this case, a half bridge with two IGBTs

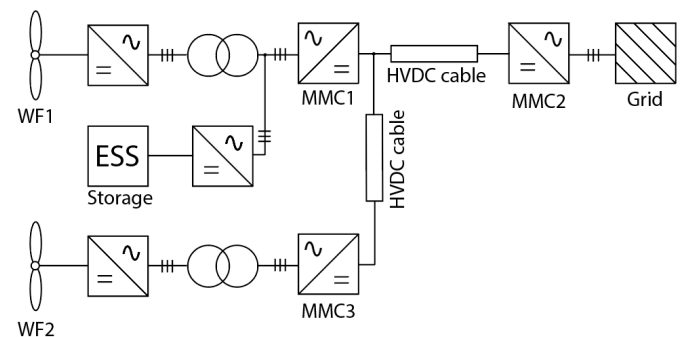


Fig. 1. Three-terminal HVDC system with offshore wind and storage integration under analysis.

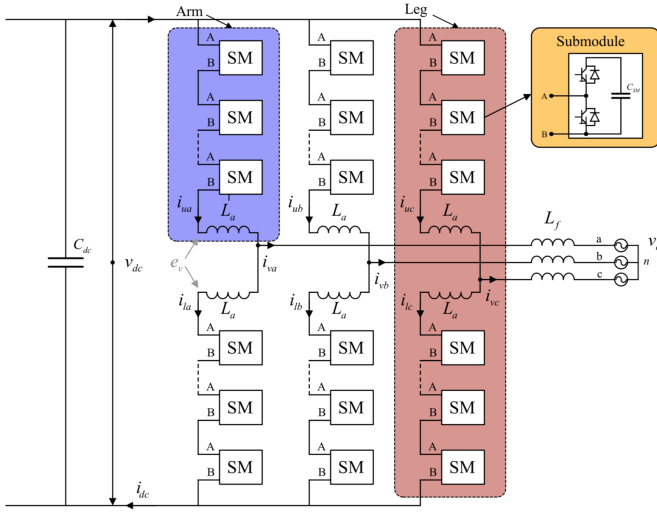


Fig. 2. A schematic of the MMC from [15].

and a capacitor. Additionally, the MMC consists of an arm inductor for each arm, L_a , and an inductor on each phase of the AC-side, L_f . The MMC is operated such that the voltage of each submodule is inserted at the output voltage in steps, resulting in a waveform close to a sine on the AC-side, e_v . The output voltage waveform is generated with respect to the grid voltage, represented by voltage sources in the schematic, to produce a flow of active and reactive power across the grid side inductors.

In [14], a comparison of all available MMC models in the literature with varying level of complexity was done, and the conclusion led to a recommendation for using average value models for network-level studies. Average models are more computationally efficient compared to the more accurate models, and they can reproduce the dynamics of the MMC accurately without detailed modeling of the internal structure of the MMC. Average models represent the MMC through controllable voltage and current sources on the AC and DC side, effectively meaning that effects of the pulse width modulation within the converter are averaged out over the switching period.

Furthermore, in this paper, the contribution of the internally stored energy in the MMC is studied. Therefore, an energy-based MMC model that includes the dynamics of the internally stored energy in the MMC was chosen.

When deciding on the how to model the MMC, it was desirable that the model should have steady state time invariant (SSTI) states. SSTI states facilitate linearized state space representations for eigenvalue analysis. Although this feature was not directly utilized in this work, it still makes the model more attractive for members of the industry and researchers wishing to make use of such techniques for stability analysis or tuning purposes. Furthermore, this makes control of the model easier.

Hence, the simplified zero-sequence MMC model from [15] was chosen. The model couples states that oscillate at the

same frequency in equation sets, which are subsequently transformed into a synchronous rotating reference frame (SRF). It is assumed that the modulation indices are calculated in a manner which compensates for the oscillations in the circulating voltage, referred to as "compensated modulation" [15]. This modeling approach is of great utility when deriving energy-based MMC models that provide great insight into the energy dynamics they introduce [16].

1) *The energy-based MMC model schematic:* Figure 3 shows the overview of the circuit implementation of the model as well as the associated control schemes.

The AC-side of the MMC is represented by a stiff grid voltage, v_g^{abc} , equivalent AC resistances, $R_{eq} = R_f + \frac{1}{2}R_a$, and inductances, $L_{eq} = L_f + \frac{1}{2}L_a$, as well as a controlled voltage source, e_v^{abc} , representing the voltage driving the AC-side currents, i_v^{abc} . The currents on the AC-side are controlled by an inner vector control of the transformed dq-currents [17]. The reference for the d-current comes from the outer power controller with DC voltage droop based on the measured power, P_{dc} , and voltage, V_{dc} . Droop control allows multiple MMCs in the grid to contribute to the DC voltage regulation. In this study, only the active power of the converter was of interest, and therefore, the reference for the q-current, controlling reactive power, was set to zero for all simulations executed in this paper.

The AC- and DC-sides are coupled using an energy balance equation, which accounts for the internal energy storage capability of the MMC, by modeling the zero-sequence energy sum, $\omega_{\Sigma,z}$ based on the equivalent arm capacitance, C_{eq} . This energy is controlled using a zero-sequence energy sum controller, including a controller for the circulating current, i_{cz} .

The DC-side is modeled using a controllable voltage source for the circulating voltage, $v_{c,z}$, as well as equivalent arm resistances, $\frac{2}{3}R_a$, and inductances $\frac{2}{3}L_a$, and a DC-side capacitor, C_{dc} . The current source in fig. 3 represents, e.g., the DC current from another MMC in a point-to-point HVDC connection.

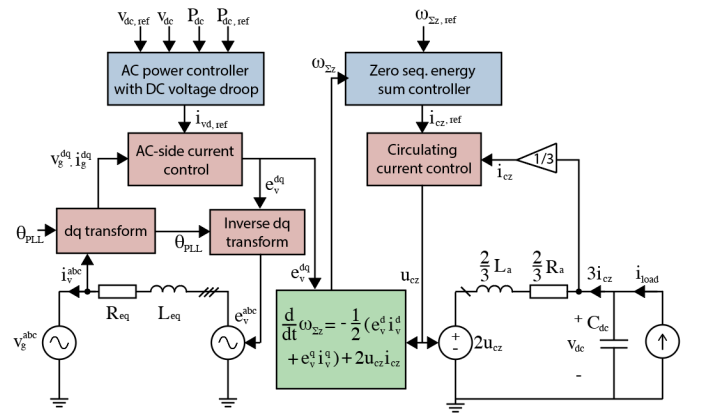


Fig. 3. Overview of the MMC model.

B. Wind farm model

The wind farm model is represented in aggregated form based on the dynamics of a single wind turbine, assuming all turbines are operated equally. Figure 4 shows a schematic including the variables used in the turbine model.

The basis for the model is the dynamic equation for torque balance between the turbine blades, T_{wind} , the electrical generator, T_{gen} , the frictional torque, $B\omega$, and the torque associated with the acceleration of the turbine and generator $J \frac{d}{dt}\omega$ which can be expressed as follows:

$$J \frac{d}{dt}\omega = T_{wind} - T_{gen} - B\omega \quad (1)$$

where J is the total inertia in turbine and the generator and ω is the rotational speed of the turbine.

The turbine mechanical power, $P_{turbine}$, can be expressed by the turbine torque, T_{wind} , as

$$P_{turbine} = \omega T_{wind} \quad (2)$$

Alternatively, the turbine power can be expressed as a fraction of the power available in the wind through the power coefficient C_p .

$$P_{turbine} = C_p P_{wind} = C_p \frac{1}{2} \rho A u^3 \quad (3)$$

where ρ is the air density, A is the area swept by the blades and u is the wind speed.

When considering the aerodynamics of the turbine blades, it is useful to define the tip speed ratio λ as:

$$\lambda = \frac{\omega \ell}{u} \quad (4)$$

where ℓ is the length of the turbine blades.

The power coefficient represents the aerodynamics of the turbine blades, and it can be expressed as a function of the tip speed ratio λ and the blade angle β representing the pitch of the blades [18]:

$$C_p(\lambda, \lambda_{ai}, \beta) = 0.5176 \left(\frac{116}{\lambda_{ai}} - 0.4\beta - 5 \right) \exp\left(\frac{-21}{\lambda_{ai}}\right) + 0.0068\lambda \quad (5)$$

where

$$\lambda_{ai}(\lambda, \beta) = \left(\frac{1}{\lambda + 0.08\beta} - \frac{0.035}{\beta^3 + 1} \right)^{-1} \quad (6)$$

Because this paper models the wind farm in an aggregated form, a gain representing the total number of turbines, $N_{turbines}$, is added to the power output from the model.

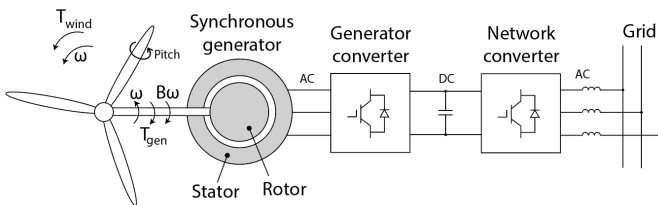


Fig. 4. A schematic of a Type IV turbine showing the basic variables used in the turbine model.

1) *Turbine controllers:* The turbine model has two control loops: one speed controller and one pitch controller.

The speed controller controls the torque of the electrical generator to regulate the speed of the turbine. This is done to maintain an optimal tip speed ratio, λ , optimizing the power coefficient, C_p , for wind conditions up to the rated wind speed, u_{rated} .

The pitch controller is activated for wind conditions above the rated wind speed. It is used to control the blade angle, β , to shed excess power when the wind speeds are above the rated value.

C. Energy storage model

The energy storage model consists of three power flows; one describing the output from the power electronics, P_{pe} , one describing the losses in the storage system, P_{loss} and one power flow that represents the power at the storage terminals, P_{es} . The equations describing the storage system are as follows:

$$P_{es} = P_{pe} + P_{loss} \quad (7)$$

$$W_{es} = \int -P_{es} \quad (8)$$

$$SOC = \frac{W_{es}}{W_{rated}} \quad (9)$$

$$0 \leq SOC \leq 1 \quad (10)$$

where SOC is the state of charge, describing how much of the total capacity the storage unit is charged, and W_{es} is the accumulated energy stored in the unit.

Two charging states of the storage unit are defined; a charging and a discharging state. The equations describing the storage unit when it is discharging are:

$$P_{pe} > 0 \quad (11)$$

$$P_{pe} = \eta \cdot P_{es} \quad (12)$$

$$P_{loss} = \left(\frac{1}{\eta} - 1 \right) \cdot P_{pe} \quad (13)$$

where η is the charging and discharging efficiency of the energy storage system, hence assumed to be equal.

Next, the equations describing the unit when it is charging are:

$$P_{pe} < 0 \quad (14)$$

$$P_{es} = \eta \cdot P_{pe} \quad (15)$$

$$P_{loss} = (\eta - 1) \cdot P_{pe} \quad (16)$$

Also, to represent the delay in the storage system, a first-order transfer function is added to the power output of the storage. The filter time constant use in this paper is $T_{delay} = 10ms$. This is a small time constant that represents a fast energy storage system as, e.g., electrochemical energy storage systems. Examples of such electrochemical energy storage systems are lithium-ion and lead-acid [19], [20].

Additionally, a storage protection system is added to limit the state of charge between 20% and 90%. Also, the protection system prevents the storage system from charging and discharging beyond the rated power.

D. HVDC cable model

The HVDC cable used for this study is a circuit representation of a frequency dependent cascaded pi-representation from [21]. This model captures the behavior of the frequency dependent parameters as resistances and inductances for a wide range of frequencies in addition to the effects of the hyperbolic correction factors in an actual cable. These aspects can be crucial in long cable implementations such as those used in offshore applications.

Figure 5 shows the cable model used, with 5 pi-sections and 3 parallel branches. The cable parameters in the Appendix were distributed to the five pi-sections by multiplying the per kilometer value with the length and then dividing by five, such that, for example, $R_1 = R_{1l} \cdot l/5$, where l is the length of the cable and R_{1l} is the parameter found in the Appendix.

IV. SIMULATION CASES AND RESULTS

A. Simulation case 1: Contribution of the MMC through the internal storage

Since the MMC contains several submodules connected in cascade, each comprising a capacitor, the MMC has some energy storage capability characterized by short charge and discharge periods. Control of this stored energy could thus be executed to improve power dynamics that occur over relatively short periods ranging from milliseconds to a couple of seconds depending on the energy requirement.

To investigate the support capability of the MMC with regards to power dynamics, two test cases were simulated. In the first test-case, the MMC attempts to smoothen out power variations arising from the turbine dynamics caused by wind speed fluctuation. In the second, the MMC attempts to reduce the response time of the HVDC system upon a step in power reference.

1) *Responding to turbine dynamics:* To investigate the improving impact an MMC can have on the power dynamics of a wind turbine caused by wind speed fluctuation, this aspect of fig. 1 was investigated using the isolated sub-system, corresponding to the model depicted in fig. 6.

The wind speed was varied around the rated wind speed of the controllers with a maximum variation of $0.2m/s$ to induce power fluctuation relating to the turbine dynamics. The controller used to determine $w_{\Sigma,z,ref}$ was a PI controller, taking $P_{WF} - P_{ref}$ as input. To ensure that the controller did not deplete the capacitors, the admissible energy range was determined to be $0.7 \leq w_{\Sigma,z,ref} \leq 1.3$. The simulation was run twice. The first time the aforementioned control was

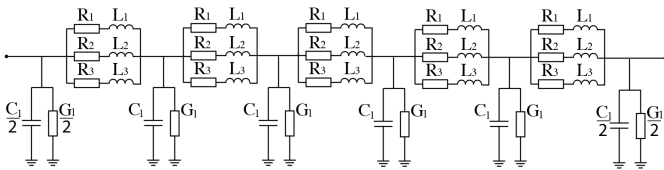


Fig. 5. Cascaded pi-representation of an HVDC cable with 5 pi-sections and 3 parallel branches.

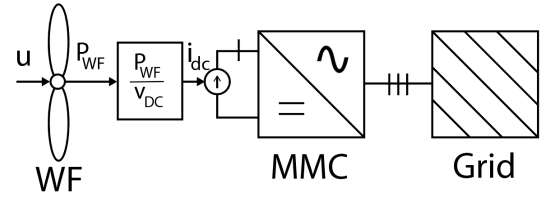


Fig. 6. Test case used to isolate the power dynamics of the turbine and MMC for Simulation case 1.

implemented and in the second, $w_{\Sigma,z,ref}$ was set equal to 1, i.e. no contribution from the internal storage in the MMC.

2) *Results:* The power delivered to the grid, together with the p.u. wind speed and rotational speed of the wind turbine, are depicted in fig. 7.

The most interesting section of this power dynamic is for $30s \leq t \leq 35s$. During this period, the wind speed increases from below the rated value, i.e. the threshold value for the pitch controller, to above the threshold value. Upon crossing this threshold, the turbine operation is changed from speed control to pitch control. The pitch angle controller is activated to shed the excess power. However, because of the delay of 1 second associated with the pitching of the blade angles, for a small time period, this extra power is fed into the converter. Additionally, the speed controller decelerates the angular velocity of the turbine releasing some of its kinetic energy.

When $w_{\Sigma,z,ref}$ is kept constant at 1 pu, this power fluctuation flows directly through the converter without being absorbed. However, when the converter is allowed to vary $w_{\Sigma,z,ref}$, this excess energy is absorbed by the converter, (fig. 8). This dampens the power fluctuation by reducing the fluctuation from 0.009 p.u to 0.006 p.u.

Subsequently, while $t \leq 48s$ the wind speed increases and decreases within the same control region. When the wind speed increases the converter absorbs energy and when the wind speed falls the converter releases energy, as shown in fig. 8. However, the time periods are so long that this energy absorption (and release) only manifests as a negligible impact on the power response, see fig. 7.

When $48s \leq t \leq 54s$, the wind speed is reduced below the threshold value, and the speed controller is activated. Thus, the rotational speed of the turbine decelerates releasing

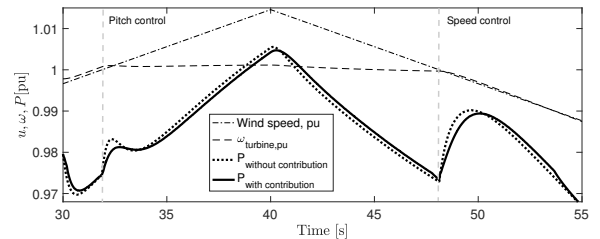


Fig. 7. Response of the powers delivered to the grid with and without contribution from the MMCs internal storage for Simulation case 1.

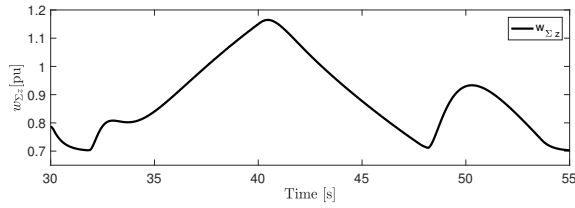


Fig. 8. Response of the internal stored energy in Simulation case 1.

some of the rotational kinetic energy stored in the inertia of the turbine to be converted and released as electrical energy into the converter. Once again, the energy absorption only causes negligible impact on the power profile. Afterwards, the converter has reached its lower energy limit and cannot release more energy. Therefore, the two power profiles converge.

3) *Response to steps in power reference:* To investigate if the MMC could improve the power step response of the HVDC system, the sub-system depicted in fig. 9 was analyzed.

MMC2 controls the power flow to Grid 3. A step in power reference from 0.7 to 0.8 was executed at $t = 1$ s. The simulations were run twice. During the first simulation $w_{\Sigma,z,ref}$ was controlled by a PI controller and in the second $w_{\Sigma,z,ref}$ was set equal to 1.

4) *Results:* Figure 10 shows the difference in response of the internal energies of the MMC when using the two control strategies.

The p.u. powers delivered to Grid 3 are displayed in fig. 11 with and without control of $w_{\Sigma,z,ref}$, thereby with and without contribution from the MMCs internally stored energy.

As can be seen, when the energy controller controls $w_{\Sigma,z,ref}$ to release energy upon a step in the power reference, the stored converter energy starts to decline and the output power of the converter reaches the power level around its reference faster than when $w_{\Sigma,z,ref}$ is set constant to 1 pu.

In both cases, $w_{\Sigma,z,pu}$ declines upon the step, causing the power leaving the converter to exceed the power entering the converter from the HVDC cable. However, when $w_{\Sigma,z,ref}$ is maintained at 1, the rate of change of the converter energy declines after 1 ms. Therefore, the difference between the power delivered to the grid and the power entering the converter

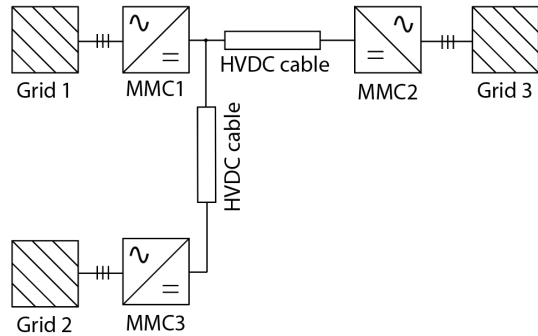


Fig. 9. System build to investigate MMC induced improvements of power step responses of HVDC systems for Simulation case 1.

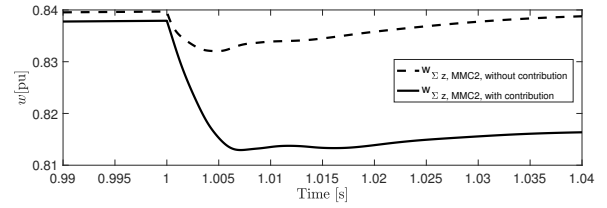


Fig. 10. Response of the stored energy in the MMC for Simulation case 1.

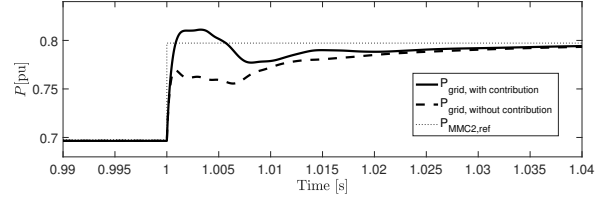


Fig. 11. Response of powers in the system for Simulation case 1.

decreases, until the converter starts to recharge at $t = 4.3$ ms after the step. Because of the recharging of the converter, there is some additional delay before the converter output energy rises again, but subsequently, it exponentially approaches its reference. When $w_{\Sigma,z,ref}$ is controlled, the power delivered to the grid overshoots and subsequently oscillates below its reference. This oscillatory behaviour was reduced in [13], by releasing the energy in an exponentially decaying manner based on the size of the step in power reference. This reduced the overshoot from 14% of the step size to 6% of the step size and reduced the undershoot by almost 3 orders of magnitude.

This simulation shows that control of the zero-sequence energy can reduce the power step response time of the HVDC system.

B. Simulation case 2: Energy storage dimensioning

Simulation case 2 aims at pre-sizing the energy storage system before it is integrated into the three-terminal HVDC system in Simulation case 3. Simulation case 2 uses a configuration where the power from the wind farm is filtered through a large first order filter, as shown in fig. 12. The difference between the filtered power and the actual power is sent as a reference for the energy storage system. This way, the combined power from the wind farm and the energy storage will have a much smoother profile than the power from the wind farm alone when the energy storage and the filter are properly dimensioned.

To dimension the energy storage rated power, the real wind speed profile shown in fig. 13 was used. These are actual wind speed data measured at Roosevelt station over approximately 20 hours.

1) *Results:* Figure 14 shows the power from WF1, the power from the energy storage, and the combined storage and wind farm power output after dimensioning of the energy storage rated power and the filter time constant.

These results and the interaction between the wind farm and the energy storage were considered satisfactory and led to the

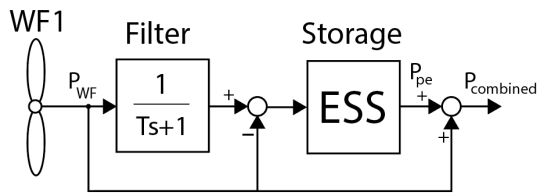


Fig. 12. Simulation setup for Simulation case 2.

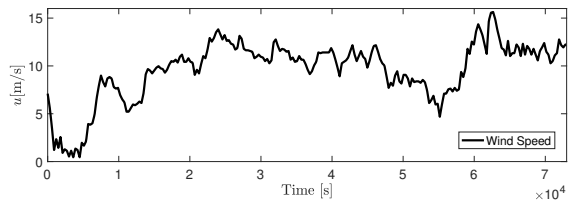


Fig. 13. The wind speed variation used for dimensioning.

deterministic choice of a P_{rated} of 250MW for the energy storage, assuming a time constant of $T = 1000s$ for the first order filter used to filter the power output from the wind farm.

Additionally, the state of charge was used as an indicator during the process of finding the rated values. From fig. 15, it can be seen that the state of charge varies in the whole range between its limits of 0.2 and 0.9 without capping at the limits during the simulation. This was regarded as an indicator that the storage was not over- nor under-dimensioned, resulting in proper utilization of the available capacity.

C. Simulation case 3: Three-terminal HVDC system with wind power and energy storage integration

To study the short term effects of integrating an energy storage system offshore near one of the wind farms in fig. 1, the configuration of Simulation case 2 was added to WF1 and the energy storage system in the final simulation system showed in fig. 1.

The offshore AC-grids are modeled by voltage sources as stiff grids, and the power outputs from the wind farm models and energy storage model are applied at the references of their respective MMC.

Two events are introduced to study the differences in responses of the system when an event occurs at WF1 with an energy storage system nearby and WF2 without an energy storage system. A sudden drop in wind speed from 10 m/s to 5m/s is introduced first at WF1 at $t = 30s$ then at WF2 at $t = 60s$.

In this simulation case, $w_{\Sigma,z,ref}$ is kept constant at 1pu for all of the MMCs.

1) *Results:* Figure 16 shows the response of the power from WF1, WF2 and the energy storage when a sudden drop in wind speed is introduced. From the figure, it can be seen how the energy storage system quickly reacts after the power from WF1 drops, to maintain a *more* constant power to MMC1.

Figure 17 shows the response of the MMC powers under the same conditions. From the figure it can be seen how the

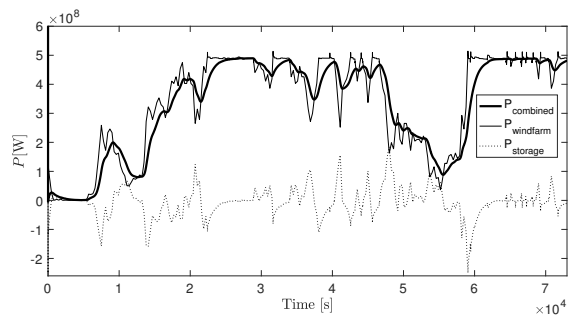


Fig. 14. Power from wind turbine, energy storage and combined power from Simulation case 2.

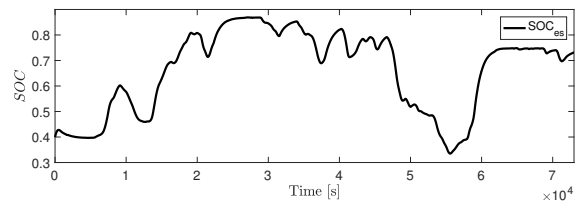


Fig. 15. The state of charge (SOC) of the energy storage from Simulation case 2.

power delivered to shore from MMC2 is *more* constant when there is a drop in wind speed at WF1 with an energy storage system compared to when there is a drop at WF2, which has no energy storage system.

Figure 18 shows the response of the DC voltages at the MMC terminals when a sudden drop in wind speed is introduced. It can be seen that the response of the DC voltages is improved for the event at WF1 at $t = 30s$ compared to the event at WF2 at $t = 60s$ due to the fast contribution of the energy storage system. In the first case, the *more* constant power output from MMC1 means that the DC voltage levels

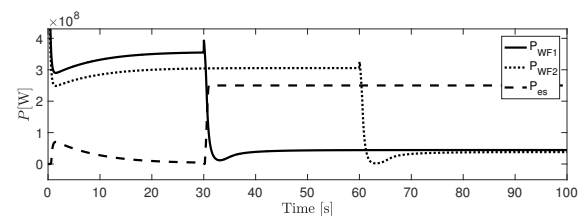


Fig. 16. The response of the wind farm powers and energy storage powers when two sudden drops in wind speed are introduced in Simulation case 3.

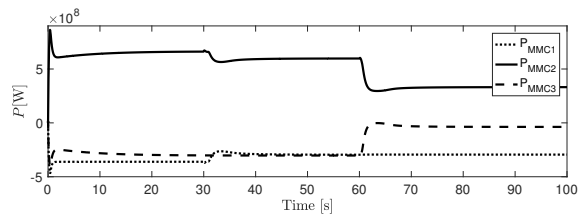


Fig. 17. Response of the MMC powers during two sudden drops in wind speeds is introduced in Simulation case 3.

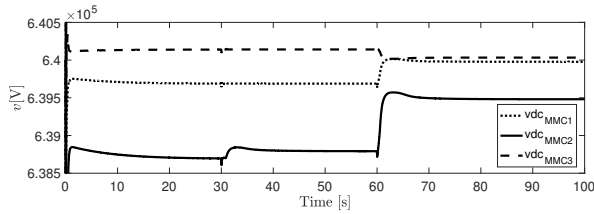


Fig. 18. The response of the DC voltages during two sudden drops in wind speeds is introduced in Simulation case 3.

do not have to be adjusted when there is a drop in the wind speed compared to the case when the wind speed drops at WF2.

Figure 19 shows the response of the zero-sequence energy sum in the MMCs when a sudden drop in wind speed is introduced. The response of the energies are also improved for the case of an event at WF1 at $t = 30$ s compared to WF2 at $t = 60$ s due to the fast contribution of the energy storage system.

V. DISCUSSION

A. The internal storage contribution of the MMC

As seen from the results, the internally stored energy in the MMCs is not large enough to account for the short term variations in the wind with the values used in this paper. However, the internal storage can be increased by either increasing the number of sub-modules in the MMC or by increasing the rated voltage of each sub-module or a combination of both.

However, because the MMC can improve fast responses as the step response of the converter, it may be beneficial to use the MMC to smooth the most rapid variations in the wind from e.g. wind gusts and tower shadowing, as studied in [8]. Possibly, these capabilities could also be used for other purposes such as power oscillation damping, improve voltage behaviour, increasing the life span of batteries by eliminating ripple or providing initial frequency response and system inertia [22]–[25].

B. Justification for offshore storage placement

In this study, the energy storage system was placed offshore near one of the wind farms. This was done to study the effects on the HVDC system when having a storage system offshore, and directly compare a wind farm complemented with energy storage to a wind farm without energy storage.

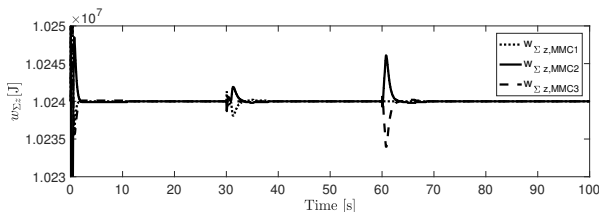


Fig. 19. The response of the zero-sequence energy of the MMCs during two sudden drops in wind speeds in Simulation case 3.

The configuration was practical for directly comparing the effects of events at both wind farms without changing the configuration of the system model.

Further, one can argue that in addition to improved operation of the HVDC system, the energy storage system can be placed offshore to fully utilize the flexibility of HVDC grids. By having the energy storage near the wind farm, the same constant power profile can be delivered regardless of the power flow direction to shore. This may be beneficial in cases where, e.g., different countries are connected by the HVDC grid. The offshore placement of the energy storage system allows the same power to flow to country x as country y , without having separate energy storage systems connected at the onshore terminals of both countries.

However, the topic of offshore versus onshore placement of the energy storage and its multiple techno-economic implications were not the main focus of this paper, and should, therefore, be addressed in separate studies.

C. Storage dimensioning

Dynamic simulations using only one wind speed series are used for pre-sizing of the energy storage system to be used further in the paper. As the dimensioning of the storage was not the main focus of this paper, the approach was chosen for its simplicity, and without presumption of generality, mainly to demonstrate one practical usage of simulations in the OpenModelica software. It should, therefore, be clarified that this approach is very simple compared to actual dimensioning of energy storage systems for real wind farms.

Also, the chosen rated power of the energy storage system was 250MW, which corresponds to around half of the rated power from the wind farm nearby, containing 70 turbines with a rated power of 7MW. The rated power from the energy storage system is therefore not enough to cover the rated power from the wind farm, and it is therefore just a complement to the wind farm production resulting in more constant operation. Economic considerations relating how this can be used to financially justify the ESS investment and considerations recommending a smaller energy storage system sizing were left outside the scope of this paper. On the other hand, the results, the results from simulation case 2 when using a rated power of the same as the wind farm did not show a good enough increase in performance to justify the potential increases in costs of a larger energy storage system.

D. Using OpenModelica for real-time HIL testing

To further address the usage of the OpenModelica for model sharing through the Functional Mock-up Interface (FMI) standard and usage in real-time HIL testing, preliminary testing was performed at the National Smart Grid laboratory in Trondheim. A review of the available literature revealed the lack of information on how to build and prepare OpenModelica models for one of Opal-RT's real-time simulators, ePHASOR-SIM. However, a short guide inside the software was found, but this guide lacked some important details. Therefore, this aspect was investigated further to increase the usefulness of

the OpenModelica software in the context of modeling HVDC grids for real-time HIL testing.

Multiple models, including a model of an MMC and a point-to-point HVDC connection using MMCs were implemented in OpenModelica, exported for the real-time simulator and successfully run in a larger system model with the real-time simulator. The approach is further described in [12], [13], and by following the included guide, HVDC grid models developed in OpenModelica can be used for real-time HIL simulations for future experimental validation and testing. The guide found in [12], [13] adds to the information found inside the software.

The real-time simulation models are added to the aforementioned GitHub folder for illustration purposes. However, to have complete access to all components in the model, the Opal-RT Modelica Developer library is needed. This library is handed out by Opal-RT's customer support upon request.

VI. CONCLUSIONS

In this paper, a three-terminal HVDC system with offshore wind and energy storage integration was modeled in OpenModelica, including the key components in an HVDC grid. The paper started by introducing the open source modeling software OpenModelica with a preliminary assessment of the performance of the software. The software was tested for the fast dynamics of a switching model of a 10kHz 2L-VSC with comparison to Simulink. The results showed that OpenModelica successfully reproduced these fast dynamics.

Next, the models for the MMC, the wind farms, the HVDC cables, and the energy storage system were described and a description of the simulation cases studied in the paper was presented.

The first simulation case showed that the internal energy of an MMC can improve the step response of the active power delivered to the grid from a three-terminal HVDC system. Further, the second simulation case showed that the contribution of the MMCs is very small when considering short term variations in the wind. Therefore, it is recommended to consider using the MMC for smoothing the most rapid changes in power due to wind gusts, tower shadowing, etc.

The third simulation used real wind speed data to pre-dimension an external energy storage system to smooth the hourly variations in power production due to changes in wind speeds. Lastly, the fourth and final simulation case combined the three terminal HVDC system with two wind farms and an energy storage system to study the short term effects of having an energy storage system at one wind farm. The results using a fast energy storage system showed that the overall operation of the HVDC system was improved when using an energy storage system, leading to smaller transients in the responses of the DC voltage and internal energy storage when wind speeds suddenly dropped.

Additionally, models developed in the software were tested in the National Smart Grid laboratory with Opal-RT's real-time simulator ePHASORSIM. This allows for future experimental testing and validation using HIL simulations.

All simulations were performed in the open source tool OpenModelica, and the models were made publicly available to anyone for any purpose, e.g. future studies including more HVDC terminals. This paper can be used as a reference for the use of such models.

VII. ACKNOWLEDGMENTS

The authors would like to express their gratitude towards Dr. Yongtao Yang in DNV GL for his guidance and advisory in the development of this paper and the associated Master's Theses.

REFERENCES

- [1] Wind Europe, "Wind in power 2018: Annual combined onshore and offshore wind energy statistics," 2018.
- [2] Wind Europe, "Wind energy in Europe: scenarios for 2030," 2017.
- [3] H. Björklund, "Strong winds, high yield," in ABB review - special report 60 years of HVDC. pp. 22–25, 2014.
- [4] M. P. Bahrman and B. K. Johnson, "The ABCs of HVDC transmission technologies," in IEEE Power and Energy Magazine, vol. 5, no. 2, pp. 32–44, March-April 2007. doi: 10.1109/MPAE.2007.329194
- [5] Weixing Lu and Boon-Teck Ooi, "Optimal acquisition and aggregation of offshore wind power by multiterminal voltage-source HVDC," in IEEE Transactions on Power Delivery, vol. 18, no. 1, pp. 201–206, Jan. 2003. doi: 10.1109/TPWRD.2002.803826
- [6] R. Marquardt, "Modular multilevel converter: An universal concept for HVDC-Networks and extended DC-Bus-applications," The 2010 International Power Electronics Conference - ECCE ASIA -, Sapporo, 2010, pp. 502–507. doi: 10.1109/IPEC.2010.5544594
- [7] K. Ilves, S. Norrga, L. Harnefors and H. Nee, "On energy storage requirements in modular multilevel converters," in IEEE Transactions on Power Electronics, vol. 29, no. 1, pp. 77–88, Jan. 2014. doi: 10.1109/TPEL.2013.2254129
- [8] A. Taffese, A. Endeganew, S. Sanchez, E. Tedeschi, "Reducing rapid wind farm power fluctuations using the modular multilevel converter", 2019.
- [9] D. Van Hertem, O. Gomis-Bellmunt and J. Liang, "HVDC grids", Wiley Online Library, 2016.
- [10] D. Winkle and C. Gühmann, "Hardware-in-the-Loop simulation of a hybrid electric vehicle using Modelica/Dymola," in Proceedings of the 22nd international battery, hybrid and fuel cell Electric Vehicle Symposium (EVS-22), Yokohama, Japan, pp. 1054–1063, 2006.
- [11] M. Otter, C. Schlegel and H. Elmqvist, "Modeling and realtime simulation of an automatic gearbox using Modelica," in Proceedings of ESS, pp. 19–23, Citeseer, 1997.
- [12] J. Espvik, "Modeling of multiterminal HVDC grids with renewable energy and storage integration by open source tools for HIL applications", M.S. thesis, Norwegian University of Science and Technology, Trondheim, June 2019.
- [13] E. Tranulis, "Modeling MMC energy dynamics in offshore HVDC systems using OpenModelica", M.S. thesis, Norwegian University of Science and Technology, Trondheim, June 2019.
- [14] S. Khan, E. Tedeschi, "Modeling of MMC for fast and accurate simulation of electromagnetic transients: a review," in Energies, vol. 10, no. 8, 2017. doi: 10.3390/en10081161
- [15] G. Bergna-Diaz, J. A. Suul and S. D'Arco, "Energy-based state-space representation of modular multilevel converters with a constant equilibrium point in steady-state operation," in IEEE Transactions on Power Electronics, vol. 33, no. 6, pp. 4832–4851, June 2018. doi: 10.1109/TPEL.2017.2727496
- [16] G. Bergna, J. A. Suul and S. D'Arco, "State-space modelling of modular multilevel converters for constant variables in steady-state," 2016 IEEE 17th Workshop on Control and Modeling for Power Electronics (COMPEL), Trondheim, 2016, pp. 1–9. doi: 10.1109/COMPEL.2016.7556695
- [17] C. Bajracharya, M. Molinas, J. A. Suul, T.M. Undeland, Tore M, "Understanding of tuning techniques of converter controllers for VSC-HVDC," in Nordic Workshop on Power and Industrial Electronics (NORPIE/2008), June 9–11, 2008, Espoo, Finland, 2008.
- [18] S. Heier, "Grid integration of wind energy: onshore and offshore conversion systems", John Wiley & Sons. 2014.

APPENDIX

- [19] H. Hesse, M. Schimpe, D. Kucevic and A. Jossen, "Lithium-ion battery storage for the grid a review of stationary battery storage system design tailored for applications in modern power grids", in *Energies*, vol. 10, no. 12, 2017.
- [20] B. McKeon, J. Furukawa, Jun and S. Fenstermacher, "Advanced lead-acid batteries and the development of grid-scale energy storage systems", in *Proceedings of the IEEE*, vol. 102, no. 6, pp. 951–963, 2014.
- [21] J. Beerten, S. D'Arco and J. A. Suul, "Frequency-dependent cable modelling for small-signal stability analysis of VSC-HVDC systems," in *IET Generation, Transmission & Distribution*, vol. 10, no. 6, pp. 1370-1381, 21 4 2016. doi: 10.1049/iet-gtd.2015.0868
- [22] A. A. Taffese, E. Tedeschi and E. de Jong, "A control scheme for utilizing energy storage of the modular multilevel converter for power oscillation damping," 2017 IEEE 18th Workshop on Control and Modeling for Power Electronics (COMPEL), Stanford, CA, 2017, pp. 1-8. doi: 10.1109/COMPEL.2017.8013415
- [23] A. E. Leon, "Short-term frequency regulation and inertia emulation using an MMC-Based MTDC System," in *IEEE Transactions on Power Systems*, vol. 33, no. 3, pp. 2854-2863, May 2018. doi: 10.1109/TPWRS.2017.2757258
- [24] J. Freytes et al., "Dynamic analysis of MMC-based MTDC grids: use of MMC energy to improve voltage behavior," in *IEEE transactions on power delivery*, vol. 34, no. 1, pp. 137-148, Feb. 2019. doi: 10.1109/TPWRD.2018.2868878
- [25] I. Puranik, L. Zhang and J. Qin, "Impact of low-frequency ripple on lifetime of battery in MMC-based battery storage systems," 2018. 10.1109/ECCE.2018.8558061.
- [26] C. A. Bharadwaj and S. Maiti, "Modular multilevel converter based hybrid energy storage system," 2017 IEEE PES Asia-Pacific Power and Energy Engineering Conference (APPEEC), Bangalore, 2017, pp. 1-6. doi: 10.1109/APPEEC.2017.8308983

TABLE I
SYSTEM PARAMETERS

Component	System parameters		
	Parameter	Value	Unit
MMC	S_n	1059	MVA
MMC	V_n	333	kV
MMC	$R_{a,pu}$	0.005	p.u.
MMC	$R_{f,pu}$	0.00285	p.u.
MMC	$L_{a,pu}$	0.08	p.u.
MMC	$L_{f,pu}$	0.16428	p.u.
MMC	$C_{eq,pu}$	0.8	p.u.
MMC	$C_{DC,pu}$	0.051637	p.u.
HVDC cable	C_l	0.1983	$\mu\text{F}/\text{km}$
HVDC cable	G_l	$7.6330 \cdot 10^{-11}$	S/km
HVDC cable	R_{1l}	$1.1724 \cdot 10^{-1}$	Ω/km
HVDC cable	R_{2l}	$8.2072 \cdot 10^{-2}$	Ω/km
HVDC cable	R_{3l}	$1.1946 \cdot 10^{-2}$	Ω/km
HVDC cable	L_{1l}	$2.2861 \cdot 10^{-1}$	mH/km
HVDC cable	L_{2l}	1.5522	mH/km
HVDC cable	L_{3l}	3.2943	mH/km
HVDC cable	l	100	km
Turbine	P_{rated}	7	MW
Turbine	J	$4 \cdot 10^6$	kgm^2
Turbine	B	$2 \cdot 10^6$	$\text{sN}^{-1}\text{m}^{-1}$
Turbine	ℓ	75	m
Turbine	ρ	1.2	kgm^{-3}
Turbine	λ_{opt}	8.1	p.u.
Turbine	C_{pmax}	0.48	p.u.
Turbine	u_{rated}	11.14	ms^{-1}
Turbine	T_{pitch}	1	s
ESS	P_{rated}	250	MW
ESS	t_{rated}	1	hour
ESS	η	0.9304	hour
ESS	$SOC_{lim,upper}$	0.9	p.u.
ESS	$SOC_{lim,lower}$	0.2	p.u.
ESS	T_{delay}	10	ms